Silicon Location in Silicate-Substituted Calcium Phosphate Ceramics Determined by Neutron Diffraction

ARTICLE *in* CRYSTAL GROWTH & DESIGN · JULY 2011

Impact Factor: 4.89 · DOI: 10.1021/cg200587s

5 AUTHORS, INCLUDING:

Jean-Marie Nedelec
Ecole Nationale Supérieure de Chimie de Cle…
156 PUBLICATIONS **1,795** CITATIONS

SEE PROFILE

Guillaume Renaudin
Ecole Nationale Supérieure de Chimie de Cle…
92 PUBLICATIONS **1,825** CITATIONS

SEE PROFILE

CRYSTAL GROWTH & DESIGN

ARTICLE

pubs.acs.org/crystal

Silicon Location in Silicate-Substituted Calcium Phosphate Ceramics Determined by Neutron Diffraction

Sandrine Gomes,[†,‡] Jean-Marie Nedelec,[†,‡] Edouard Jallot,[§] Denis Sheptyakov,[#] and Guillaume Renaudin*[,†,‡]

[†]Clermont Université, ENSCCF, Laboratoire des Matériaux Inorganiques, BP 10448, 63000 Clermont-Ferrand, France

[‡]CNRS, UMR 6002, LMI, 63177 Aubière, France

[§]LPC, Clermont Université, UBP/CNRS, Clermont-Ferrand, France

[#]Laboratory for Neutron Scattering, Paul Scherrer Institut, 5232 Villigen PSI, Switzerland

ABSTRACT: The silicate incorporation in calcium phosphate bioceramics was studied by X-ray and neutron powder diffraction (joint Rietveld refinement) and micro-Raman spectroscopy. For a phosphate substitution level of 15 mol % multiphase ceramic is obtained passing from biphasic calcium phosphate (BCP) ceramic to ceramic composed of hydroxyapatite (HAp), silicocarnotite, and tricalcium phosphate (both α- and β-TCP polymorphs). The quantity of silicate incorporation increases when passing from β-TCP ($Ca_3(PO_4)_2$, silicate level not measurable) to α-TCP ($Ca_3(PO_4)_{1.875}(SiO_4)_{0.125}$ with 6.25 mol % of phosphate substitution or 1.13 wt % of incorporated silicon), to HAp ($Ca_{10}(PO_4)_{4.9(2)}(SiO_4)_{1.1(2)}(OH)_{1.0(1)}O_{0.66(7)}$ with 18.3 mol % of phosphate substitution or 3.11 wt % of silicon), and to silicocarnotite ($Ca_5(PO_4)_{1.9(2)}(SiO_4)_{1.1(2)}$ with 36.7 mol % of phosphate substitution or 6.40 wt % of silicon). The mechanism of silicate incorporation into HAp structure is multiple and involves the creation of two kinds of vacancies: hydroxyl vacancies and phosphate/silicate vacancies due to a carbonate-involving mechanism leading to the composition $Ca_{10}(PO_4)_{6-x-2y}(SiO_4)_{x+y}(\square_T)_y(OH)_{2-x}O_y\square_{x-y}$. The formation of important hydroxyl vacancies in the hexagonal channel of the HAp structure leads to the stabilization of silicocarnotite (that can be considered as a polymorph of the highly Si-substituted HAp phase). The $Ca_{10}(PO_4)_{4.9(2)}(SiO_4)_{1.1(2)}(OH)_{1.0(1)}O_{0.66(7)}$ composition appears then to be the end-member of the hexagonal Si-HAp solid solution. Silicocarnotite is formed above this silicate insertion level.

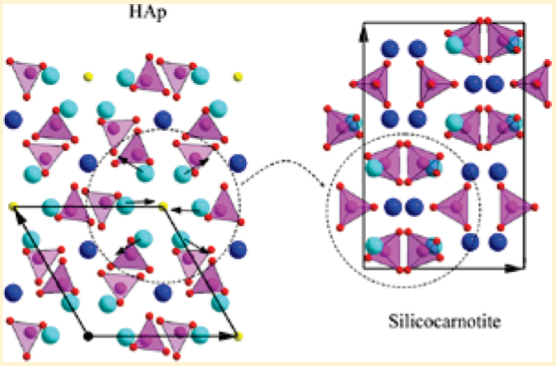

1. INTRODUCTION

It is well-known that bone mineral mass is dominated by nanocrystalline, nonstoichiometric hydroxyapatite (HAp, $Ca_{10}(PO_4)_6(OH)_2$), and whitlockite, the Mg-incorporated β-tricalcium phosphate (β-TCP, β-$Ca_3(PO_4)_2$), can be found at many different sites in the human body.[1−3] For these reasons and because of the difference in the solubility of the two calcium phosphate phases, biphasic calcium phosphates (BCP), composed of a mixture of HAp and β-TCP, are interesting biocompatible materials for reconstructive surgery and for bone prosthesis coatings.[4−7] Calcium phosphate based bioceramics are widely used as powders or granulates to fill and restore small bone defects.[8] The bioactive behavior of HAp can be improved by introducing substitutions into the structure. Actually, the HAp structure can incorporate a wide variety of ions that can affect both cations and anions, with the same oxidation state (such as Sr^{2+},[9,10] Mg^{2+},[11] Zn^{2+},[12] F^-,[13] Cl^-,[14] etc., ...) and with different oxidation states.[15−17] One of the alternatives to improve the properties of crystalline calcium phosphates is to incorporate silicon into the crystal structures.[18−21] Si, an essential trace element required for healthy bone and connective tissue, influences the biological activity of Si-substituted calcium phosphate bioceramics.[21−23] Recent reviews of Bohner[24] and Habibovic and Barralet[25] state it is not presently clear if and how Si substitution positively influences the biological response of Si-substituted calcium phosphate.

The first step to identify the silicon biological effect is to clearly characterize the prepared Si-incorporated materials: number and nature of the crystalline phases, presence of amorphous silica-gel, location of silicate anions in the crystallographic structures or included in a fairly soluble compound, and mechanisms of silicate insertion. The lack of products characterization (what really is behind the term "silicate-substituted calcium phosphate") was a problem to understand the real influence of Si on the biological behavior of Si-substituted calcium phosphate ceramics.[24] It appears from the literature (as reported by Palard et al.[26]) that the preparation of single phase crystallized Si-HAp sample is still a difficulty, indicating that the mechanism of silicate incorporation is not trivial. Several authors have studied the mechanism of silicon incorporation into the HAp structure.[18,27−30] It is widely

Received: May 9, 2011
Revised: June 17, 2011
Published: July 11, 2011

assumed, and also demonstrated,[30,31] that the Si atom (or SiO_4^{4-} tetrahedra) replaces the P atom (or PO_4^{3-} tetrahedra) with the subsequent charge imbalance. According to the authors and according to the methods used for the synthesis of Si-HAp: (1) several mechanisms to reach the electroneutrality of Si-HAp have been proposed, (2) the maximal percentage of Si-incorporation differs (from 1.6 wt %[27] to 4.0 wt %[32]), and (3) samples are single- or multiphased (containing either β-TCP or α-TCP, and also silicocarnotite of composition $Ca_5(PO_4)_2SiO_4$). Several methods for the synthesis of Si-HAp have been described, including the sol−gel method,[33] the hydrothermal synthesis,[32,34] the solid-state reactions,[35,36] and the more generally encountered aqueous precipitation method.[26−30,37−40] It appears from recent studies that the basically assumed charges compensation

$$PO_4^{3-} + OH^- \leftrightarrow SiO_4^{4-} + \square_{OH} \quad \text{(ref 18)}$$

(with $\square_{OH}$ an hydroxyl vacancy), leading to the generally assumed composition $Ca_{10}(PO_4)_{6-x}(SiO_4)_x(OH)_{2-x}$ for Si-HAp, is not so evident. Other more complex rules for charges compensation have been proposed:

$$PO_4^{3-} + O^{2-} \leftrightarrow SiO_4^{4-} + OH^- \quad \text{(ref 36)}$$

$$2PO_4^{3-} \leftrightarrow SiO_4^{4-} + HPO_4^{2-} \quad \text{(ref 36)}$$

$$\square_{Ca} + 2PO_4^{3-} \leftrightarrow Ca^{2+} + 2SiO_4^{4-} \quad \text{(ref 30)}$$

$$\square_{Ca} + PO_4^{3-} + OH^- \leftrightarrow Ca^{2+} + SiO_4^{4-} + O^{2-} \quad \text{(ref 30)}$$

(with $\square_{Ca}$ a calcium vacancy). Charges compensation rules taking into account additional ionic entities have also been considered, for example, cations such as alkalines or rare earths,[35] or anions such as carbonates.[18,26,29,32,37] Palard et al.[26] have demonstrated the role played by carbonate for the synthesis of single phase Si-HAp (previously assumed by Arcos et al.[37]) and proposed the following charge balances:[26]

$$CO_3^{2-} + SiO_4^{4-} \leftrightarrow 2PO_4^{3-} \quad \text{(ref 26)}$$

$$yCO_3^{2-} + yCa^{2+} + (x-y)SiO_4^{4-} \leftrightarrow xPO_4^{3-} + y\square_{Ca} + xOH^- \ (\textit{with } y < 0.5) \quad \text{(ref 26)}$$

The present study aims to investigate in depth the mineralogy of Si-substituted multiphased calcium phosphate ceramics in order to better determine the localization of silicon within the crystallographic structures of the different calcium phosphate phases and to better characterize the Si-HAp compound. Because of the lack of electronic contrast between P and Si for X-ray diffraction experiments (possessing a ratio of ~1.07 only in X-ray scattering factors), high resolution−high intensity neutron diffraction experiments have been performed to differentiate Si from P located in the same crystallographic sites (having a higher ratio of ~1.24 in their bound coherent neutron scattering lengths with 5.13 fm for P and 4.15 fm for Si) allowing the quantitative determination of the silicon substitution into phosphate compounds.

2. MATERIALS AND METHODS

2.1. Elaboration of Si-Inserted Calcium Phosphate Ceramics. Samples of nominal composition $Ca_{10}(PO_4)_{6-x}(SiO_4)_x(OH)_{2-x}$ with x = 0.0, 0.5, and 1.0 have been synthesized using the aqueous precipitation method.[18] The previously used synthesis protocol using the aqueous precipitation led to crystallized samples without amorphous silica-gel.[30] The starting materials used were calcium hydroxide ($Ca(OH)_2$, Riedel-de Haën), orthophosphoric acid (H_3PO_4, Sigma-Aldrich), and silicon acetate ($Si(CH_3COO)_4$, Aldrich). The synthesized samples are named Si_x-CP (for Si-substituted calcium phosphates) with x being the value of the nominal silicate substitution considering the HAp composition (x = 0.0, 0.5, and 1.0). The appropriate quantities of reactants to prepare Si_x-CP were calculated by assuming that silicate would substitute for phosphate according to the mechanism $PO_4^{3-} + OH^- \leftrightarrow SiO_4^{4-} + \square_{OH}$ to ensure charge balance. Special care was applied for the highly hygroscopic H_3PO_4 manipulation, namely, for weighting. The precipitation reactions were carried out at room temperature under stirring, and the pH was maintained at 10.5−11 by the addition of ammonium hydroxide solution. After reactants were mixed, the suspension was aged overnight. The resulting precipitate was filtered and dried overnight at 80 °C. The three as-prepared powders were heated at 1100 °C for 15 h.

2.2. X-ray Powder Diffraction (XRPD). XRPD patterns were recorded on an X'Pert Pro PANalytical (Almelo, Netherlands) diffractometer, with $\theta-\theta$ geometry, equipped with a X-Celerator detector, and using Cu Kα radiation (λ = 1.54184 Å). XRPD patterns were recorded at room temperature in the interval $4° < 2\theta < 138°$, with a step size of $\Delta 2\theta = 0.0092°$ and a counting time of 100 s for each data value. A total counting time of about 250 min was used for each sample. The patterns showed samples were multiphased: $Si_{0.0}$-CP and $Si_{0.5}$-CP contain HAp (large majority) and β-TCP, whereas $Si_{1.0}$-CP was composed of the four HAp, β-TCP, α-TCP, and silicocarnotite phases.

2.3. Neutron Powder diffraction (NPD). NPD experiments were performed with the high resolution−high intensity HRPT diffractometer[41] at SINQ/PSI (Villigen, Switzerland) at room temperature. The samples (~3 g mass) were enclosed in cylindrical vanadium containers of ~8 mm diameter and measured at two different wavelengths (λ = 1.494 and 1.886 Å) in the 2θ range 4−165° with a step size of $2\theta = 0.05°$. The transmission factor was calculated ($\mu R = 0.20$) and data were corrected accordingly. The patterns showed the same phases as those observed by X-ray diffraction. The low amount of hydrogen atoms in the samples allows recording NPD patterns with acceptable background without preparing deuterated samples. The use of high resolution−high intensity neutron diffractometer is needed to refine Si atoms in calcium phosphate phases because the Si atom presents a weak neutron scattering contrast and no X-ray scattering contrast with the P atom. The high neutron scattering contrast of hydrogen atoms, due to its negative neutron scattering length of −3.74 fm, allows its localization and site occupancies refinement with good accuracy (necessary for the OH^-, O^{2-}, and vacancies populations into the hydroxyl site of the HAp structure).

2.3. Rietveld Analyses. Joint Rietveld refinements based on the simultaneous use of one X-ray pattern (λ = 1.54184 Å) and two neutron patterns (λ = 1.494 and 1.886 Å) were performed for each sample with the program FullProf.2k Multi-Pattern.[42] This technique allows reaching good accuracies in the refinement of Ca, Si, P, O, and H sites (site positions and site occupancies). The initial structural parameters of hydroxyapatite, $Ca_{10}(PO_4)_6(OH)_2$, were taken from ref 43: space group $P6_3/m$, Z = 1, a = 9.432 Å, and c = 6.881 Å, two Ca (Ca1 in 4*f*, Ca2 in 6*h*), one P in 6*h*, four O (O1 and O2 in 6*h*, O2 in 12*i* and O4 in 4*e*) and one H1 in 4*e* (O4 and H1 positions in site 4*e* − the hydroxyl anion − are half occupied due to splitting around the site 2*a*). The initial structural parameters of β-TCP, $Ca_3(PO_4)_2$, were taken from ref 44: space group *R*3*c*, Z = 21, a = 10.4352 Å, and c = 37.4029 Å, five Ca (Ca1 to Ca3 in 18*b*, Ca4 and Ca5 in 6*a* with Ca4 having a partial occupancy factor), three P (P1 in 6*a*, P2 and P3 in 18*b*), and 10 O (O1 to O9 in 18*b* and O10 in 6*a*). The

Table 1. Nominal (Synthesis), Experimental (Determined by ICP-AES) and Refined (Extracted from Rietveld Analyses) Compositions[a]

		composition (wt %)				
sample		CaO	P_2O_5	SiO_2	Ca/(P + Si)	x[b]
$Si_{0.0}$-CP	nominal	56.84	43.16		1.67	0.0
	experimental	57(3)	43(2)		1.7(2)	0.0(−)
	refined	56(1)	43(2)		1.6(1)	0.0(−)
$Si_{0.5}$-CP	nominal	57.16	39.78	3.06	1.67	0.5
	experimental	57(3)	40(2)	2.8(1)	1.6(2)	0.47(2)
	refined	56(1)	40(2)	2.7(1)	1.7(2)	0.45(2)
$Si_{1.0}$-CP	nominal	57.48	36.36	6.16	1.67	1.0
	experimental	57(3)	37(2)	6.0(3)	1.6(2)	0.97(4)
	refined	56(2)	36(3)	6.9(6)	1.6(3)	1.1(1)

[a] Standard deviations are indicated in parentheses (5% estimated for ICP-AES analyses). [b] x value corresponding to the composition $Ca_{10}(PO_4)_{6-x}(SiO_4)_x(OH)_{2-x}$.

initial structural parameters of α-TCP, $Ca_3(PO_4)_2$, were taken from ref 45: space group $P2_1/a$, Z = 24, a = 12.887 Å, b = 27.280 Å, c = 15.219 Å, and β = 126.20°, 78 independent atomic positions all in 4*e* (18 Ca, 12 P, and 48 O). And the initial structural parameters of silicocarnotite, $Ca_5(PO_4)_2SiO_4$, were taken from ref 46: space group *Pnma*, Z = 4, a = 6.737 Å, b = 15.508 Å, and c = 10.132 Å, three Ca (Ca1 in 4*c*, Ca2 and Ca3 in 8*d*), one P1 in 4*c*, one P2/Si1 in 8*d* (50%−50% statistic distribution) and seven O (O1 and O2 in site 4*c*, O3 to O7 in 8*d*).

In the course of the refinement, a supplementary hydrogen position was considered for the HAp phase: the hydrogen atom belonging to the HPO_4^{2-} anion in site 6*h* (x = 0.4746, y = 0.1666)[36] with a very small occupancy factor in order to check its presence or absence. The following parameters were first refined: scale factors, zero shifts, line profile parameters, lattice parameters, preferential orientations, and asymmetry parameters. In a second step, thermal displacement factors were refined as well as atomic coordinates when allowed by a sufficient weight percent of the phase (HAp for the three samples, and silicocarnotite for sample $Si_{1.0}$-CP). Four thermal displacement factors were considered: one for Ca, one for P/Si, one for O from phosphate groups, and one for the hydroxyl group (O and H sites from hydroxyl were constrained together in order to avoid strong correlation between thermal displacement and occupancy parameters). The silicon substitution for P sites was refined for HAp and silicocarnotite and not for the two TCP polymorphs (due to their lower weight amounts and their numerous P atomic positions). The calcium site occupancies of HAp structure converged to unity for the three samples. The procedure used (both data-collection and refinement strategy) corresponds to the general guidelines for structure refinement using the Rietveld (whole-profile) method formulated by the International Union of Crystallography Commission on Powder Diffraction.[47]

2.4. Raman Spectroscopy. Micro-Raman spectra were recorded at room temperature using a Jobin-Yvon T64000 device. The spectral resolution obtained with an excitation source at 514.5 nm (argon ion laser line, Spectra Physics 2017) is about 1 cm^{-1}. The Raman detector was a charge coupled device (CCD) multichannel detector cooled by liquid nitrogen to 140 K. The laser beam was focused onto the sample through an Olympus confocal microscope with 10× (whole sample) and 100× (selected region) magnifications. Measured power at the sample level was kept low (less than 10 mW) in order to avoid any damage to the material. The Raman scattered light was collected with the microscope objective at 180° from the excitation and filtered with an holographic Notch filter before being dispersed by a single grating (1800 grooves per mm). Spectra were recorded in the frequencies ranges 150−1500 cm^{-1} and 3000−3800 cm^{-1} in order to investigate respectively the Raman active vibration modes of phosphate−silicate tetrahedra and hydroxyl stretching.

3. RESULTS

3.1. Mineralogical Characterization. The chemical compositions of all the samples were determined by inductively coupled plasma atomic emission spectroscopy (ICP-AES). The nominal and experimental compositions of the three samples are listed in Table 1. The achieved experimental compositions agree with the targeted nominal ones (see experimental x values and Ca/(P + Si) ratios). Figure 1 shows the joint Rietveld plots obtained for $Si_{0.5}$-CP (biphasic example) and for $Si_{1.0}$-CP (multiphasic example) samples. Experimental Rietveld parameters are gathered in Table 2 and main Rietveld results are gathered in Table 3. Refined compositions of the three samples extracted from Rietveld analyses are indicated in Table 3. Correspondance between experimental and refined Ca/(P + Si) and x values guarantees the accuracy of Rietveld treatments (see Table 1).

Undoped $Si_{0.0}$-CP and Si-doped $Si_{0.5}$-CP samples are biphasic calcium phosphate ceramics composed of HAp and β-TCP phases. These two samples contain a large majority of HAp phase: 95 wt % for $Si_{0.0}$-CP and 90 wt % for $Si_{0.5}$-CP (see Table 3). Highly doped $Si_{1.0}$-CP sample is composed of four phases: HAp (32 wt %), silicocarnotite (31 wt %), α-TCP (23 wt %), and β-TCP (14 wt %). Chemical formula of silicocarnotite $Ca_5(PO_4)_2SiO_4$ corresponds to Si-HAp chemical formula $Ca_{10}(PO_4)_{6-x}(SiO_4)_x(OH)_{2-x}$ with x = 2 (the maximal physical value for x). Nevertheless, silicocarnotite has an orthorhombic structure[46] and cannot be considered as the end-member of the hexagonal Si-HAp solid solution. Because of the Si-destabilizing feature for β-TCP,[48,49] no Si insertion was considered during refinement for β-TCP. Nevertheless, it appears that a small quantity of silicate should substitute phosphate in β-TCP according to a slight increase of the lattice parameters (Table 3) and according to previous[29] Si NMR evidence.[30] The pseudobinary Ca_2SiO_4−$Ca_3(PO_4)_2$ system determined by Nurse et al.[48] gives a coarse estimation of about $Ca_3(PO_4)_{1.97}(SiO_4)_{0.03}$ for the maximal silicate insertion into the β-TCP polymorph. Above this silicate insertion level, the α-TCP polymorph is formed. The Si-insertion level into the Si-stabilized α-TCP phase was estimated by considering the refined lattice parameters correlated with the study on Si-α-TCP realized by Reid et al.[49] Our refined lattice parameters for the Si-α-TCP phase in $Si_{1.0}$-CP correspond to the maximal Si-substitution: 1.14 Si wt % for the $Ca_3(PO_4)_{1.875}(SiO_4)_{0.125}$ composition. The presence of silicocarnotite, the silicate-rich compound of the investigated CaO-PO_4−SiO_4 system, indicates that the other phases (HAp, α-TCP and β-TCP) insert their maximal quantities of silicate (considering that equilibrium has been reached after 15 h at 1100 °C).

The refined composition for silicocarnotite, $Ca_5(PO_4)_{1.9(2)}(SiO_4)_{1.1(2)}$, is very close to the normal $Ca_5(PO_4)_2SiO_4$ composition (discrepancy is within the standard deviation). Refinement of phosphorus and silicon populations into the two crystallogrtaphic P sites indicates that silicate substitution occurs in the two P1 and P2 sites (contrary to the conclusion of Dickens and Brown[46] which indicates silicate substitution in the P2 site only). The similar average interatomic distances in both

Table 2. Experimental Rietveld Parameters Indicated in the Sequence NPD (λ =1.886 Å), NPD (λ = 1.494 Å), XRPD (λ = 1.54184 Å)

sample	$Si_{0.0}$-CP	$Si_{0.5}$-CP	$Si_{1.0}$-CP
wavelength (Å)	1.886, 1.494, 1.54184	1.886, 1.494, 1.54184	1.886, 1.494, 1.54184
angular range 2θ (°)	4-165, 4-165, 4-138	4-165, 4-165, 4-138	4-165, 4-165, 4-138
N_{obs}	3218, 3218, 14634	3218, 3218, 14634	3218, 3218, 14634
N_{ref}	720, 1445, 1111	720, 1443, 1112	6750, 13022, 8106
R_p (%)	4.17, 4.11, 5.27	4.33, 4.14, 4.08	4.54, 3.96, 3.50
R_{wp} (%)	5.41, 5.26, 7.48	5.60, 5.26, 6.38	5.79, 5.04, 4.90
R_{Bragg} − Hap (%)	7.43, 9.11, 8.20	9.84, 11.4, 6.05	6.43, 7.51, 3.66
R_F − Hap (%)	6.27, 7.00, 2.57	7.64, 8.88, 4.87	4.00, 5.02, 2.45
R_{Bragg} − silicocarnotite (%)			7.59, 7.92, 3.95
R_F − silicocarnotite (%)			4.46, 5.14, 2.54
χ^2	9.4, 9.3, 8.6	7.29, 6.25, 5.32	3.51, 2.90, 4.82
global χ^2	9.2	6.39	3.74
global parameters	32	32	29
profile parameters	10	18	19
intensity-dependent parameters	23	22	57

phosphate tetrahedra (1.56 Å for the average P1−O distance and 1.57 Å for the average P2−O distance, see Table 3) agree with a similar silicon silicate substitution for the two independent phosphorus sites in silicocarnotite.

3.2. Si Substitution in HAp Structure. Figure 2 shows the evolution of the HAp lattice parameters (a and c), the tetrahedral elongation index (TEI is here defined by $(d^{max}_{P-O} - d^{min}_{P-O}/\overline{d_{P-O}}$ where d^{max}_{P-O}, d^{min}_{P-O}, and $\overline{d_{P-O}}$ denote respectively the longer, the shorter, and the average P−O distances in the phosphate tetrahedron) and the tetrahedral distortion index (TDI = $1/6\Sigma^6_{i=1}|OPO_i - OPO_m|$, with OPO_i each of the six angles between the central P atom and its four oxygen atoms, and OPO_m their average) as a function of the nominal x value. TDI was generally used to characterize the silicate substitution.[18,36,37] The three Si_x-CP samples illustrate again that the lattice parameter c is actually the best structural indicator to follow the silicate for phosphate substitution in Si-HAp.[30] The lattice parameter a is absolutely inadequate, due to non-monotonous variation. The tetrahedral indexes, TEI and TDI, seem adequate when considering these three Si_x-CP samples but fail in reproductibility when considering different synthesis series (see opened square symbols in Figure 2), contrary to lattice parameter c.

Rietveld refinements did not show calcium vacancies either in Ca1 or in Ca2 sites (occupancies converged to unity). The absence of calcium vacancies in the undoped HAp refutes a silicate insertion mechanism involving calcium-deficient HAp. The refined compositions for HAp phases in samples $Si_{0.0}$-CP and $Si_{0.5}$-CP (Table 3) indicate almost equivalent occupancies for O4 and H1 sites from the hydroxyl group. The O4 site is almost fully occupied (50% correspond to a full occupancy due to splitting around the 2a site), and the associated H1 site has an occupancy of about 40% (Table 3). Very few oxygen (from hydroxyl group) vacancies were refined, and the OH^-/O^{2-} ratio is about 2.4 for both samples. This value corresponds to the one obtained by Arcos et al. for undoped HAp but differs significantly for Si-HAp (8.75 for x = 0.33 with ceramic method).[36] This indicates that the mechanism of charges compensation is highly synthesis dependent. In the same way, Rietveld refinement indicates clearly the absence of a HPO_4^{2-} unit in our samples, contrary to results of Arcos et al.[36] The refined values of the occupancy factor of H2 site next the O2 site (located at x = 0.4746, y = 0.1666 and z = 1/4 according to Arcos et al.[36]) were −1 (4) and −1 (2) %, for $Si_{0.0}$-CP and $Si_{0.5}$-CP samples, respectively. The H2 site was not considered in sample $Si_{1.0}$-CP because of the lower weight percent of Si-HAp (32 wt %). Thus, the H2 site can be considered as empty, indicating again the importance of the mode of synthesis for the charge balance mechanism.

3.3. Si Insertion into α-, β-TCP and Silicocarnotite. The Si-stabilizing feature for α-TCP[48,49] is evidenced in sample $Si_{1.0}$-CP with a higher quantity of α-TCP (23 wt %) compared to β-TCP (14 wt %). Lattice parameters of α-TCP corroborate with the maximal silicate substitution determined by Reid et al.[49] corresponding to the $Ca_3(PO_4)_{1.875}(SiO_4)_{0.125}$ composition. Remaining Si (which was contained neither in Si-HAp, nor in β-TCP and nor in Si-α-TCP) led to the formation of a large quantity of silicocarnotite. Silicocarnotite is a solid solution which accepts small variation in the phosphate to silicate ratio.[50] Refinement of the silicate substitution in both phosphorus crystallographic sites from silicocarnotite structure[46] converges to 32% (P1) and 40% (P2) leading to the refined composition of $Ca_5(PO_4)_{1.9(2)}$-$(SiO_4)_{1.1(2)}$ close to the normal composition $Ca_5(PO_4)_2SiO_4$.

The crystallographic relationship between the hexagonal HAp and the orthorhombic silicocarnotite lattice has already been established by Keppler in 1968[51] ($a_{silicocarnotite} \approx c_{HAp}$, $b_{silicocarnotite} \approx \sqrt{3}\cdot a_{HAp}$ and $c_{silicocarnotite} \approx a_{HAp}$ with $V_{silicocarnotite} \approx 2V_{Hap}$). Our refined lattice parameters give the following ratios: $a_{silicocarnotite}/c_{HAp}$ = 0.97, $b_{silicocarnotite}/(\sqrt{3}\cdot a_{HAp})$ = 0.95, $c_{silicocarnotite}/a_{HAp}$ = 1.08, and $V_{silicocarnotite}/(2V_{HAp})$ = 0.99 indicating a relatively equivalent compactness for both structures. The crystal structure reorganization when passing from HAp to silicocarnotite structure evidence the key role played by the hydroxyl hexagonal channel in HAp and consequently the key role played by the hydroxyl vacancies to stabilize silicocarnotite. Figure 3 shows the structural relationship between the two structures. The structure relationship is far from trivial when comparing both structures. The silicocarnotite structure is built from the HAp structure when considering large amounts of hydroxyl vacancies, i.e., when considering the emptying of hydroxyl hexagonal channels (hydroxyl sites are represented by yellow spheres in Figure 3 left). The obtained

Table 3. Main Results of the Joint Rietveld Analyses (Standard Deviations Are Indicated in Parentheses)

	$Si_{0.0}$-CP	$Si_{0.5}$-CP	$Si_{1.0}$-CP
		HAp	
wt %	95 (1)	90 (1)	32 (1)
a (Å)	9.41867 (9)	9.4242 (1)	9.4106 (2)
c (Å)	6.88380 (7)	6.89517 (9)	6.9166 (2)
V (Å^3)	528.857 (9)	530.35 (1)	530.47 (2)
Si occupancy in P1 (%)[a]	−1 (4)	8 (4)	18 (4)
O4 occupancy (%)[b]	49.0 (4)	48.4 (4)	41.6 (8)
H1 occupancy (%)[b]	34.5 (8)	33.9 (8)	25 (2)
H2 occupancy (%)[c]	−1 (4)	−1 (2)	
B_{iso}(OH) (Å^2)	1.0 (1)	1.2 (1)	1.8 (1)
d_{O-H} (Å)	0.91 (1)	0.88 (1)	0.82 (3)
average $\overline{d_{P-O}}$ (Å)	1.53	1.53	1.53
TEI	0.013	0.020	0.046
average O−P−O (°)	109.45	109.44	109.41
TDI	1.59	1.81	2.35
refined composition	$Ca_{10}(PO_4)_{6.0(2)}(OH)_{1.38(4)}$ $O_{0.58(3)}\square_{0.04(2)}$	$Ca_{10}(PO_4)_{5.5(2)}(SiO_4)_{0.5(2)}$ $(OH)_{1.36(4)}O_{0.58(3)}\square_{0.06(2)}$	$Ca_{10}(PO_4)_{4.9(2)}(SiO_4)_{1.1(2)}$ $(OH)_{1.0(1)}O_{0.66(7)}\square_{0.34(4)}$
		β-TCP	
wt %	5 (1)	10 (1)	14 (1)
a (Å)	10.3642 (6)	10.3691 (3)	10.3835 (4)
c (Å)	37.186 (4)	37.162 (2)	37.253 (2)
V (Å^3)	3459.3 (5)	3460.3 (3)	3478.4 (3)
		α-TCP	
wt %			23 (1)
a (Å)			12.853 (1)
b (Å)			27.361 (1)
c (Å)			15.2240 (9)
β (°)			126.355 (6)
V (Å^3)			4311.7 (5)
		silicocarnotite	
wt %			31 (1)
a (Å)			6.7399 (2)
b (Å)			15.4341 (4)
c (Å)			10.1185 (3)
V (Å^3)			1052.57 (2)
Si occupancy in P1[d]			32 (7)
average $\overline{d_{P1-O}}$ (Å)			1.56
Si occupancy in P2[d]			40 (8)
average $\overline{d_{P2-O}}$ (Å)			1.57
refined composition			$Ca_5(PO_4)_{1.9(2)}(SiO_4)_{1.1(2)}$

[a] Silicon substitution percent in P1 site from HAp structure. [b] O4 and H1 are crystallographic sites relative to the hydroxyl group. [c] H2 is crystallographic site relative to the HPO_4^{2-} group. [d] Silicon substitution percent in P1 and P2 sites from silicocarnotite structure.

void channels destabilized the six adjacent calcium cations in Ca2 sites (cyan spheres in Figure 3 left) which pass from a seven to a six coordination number. Two of them are shifted toward the central vacancies, whereas the four others are shifted in the opposite direction to approach a phosphate tetrahedron leading to the loss of hexagonal symmetry (see arrows in Figure 3 left). Two kinds of calcium cations can be isolated in these structures: $1/Ca^{2+}$ forming chains represented by dark blue spheres in Figure 3 for both structures (Ca1 linear columns along the *c* axis for HAp, Ca1 and Ca2 zigzag chains along the *a* axis for silicocarnotite), and $2/Ca^{2+}$ which alternate with phosphate/silicate tetrahedra represented by cyan spheres in Figure 3 (Ca2 site in HAp, Ca3 site in silicocarnotite). The orthorhombic silicocarnotite structure can be obtained from the hexagonal HAp structure by replacing the hydroxyl hexagonal channel by zigzag Ca−Ca chains. The Ca1 site from HAp relates to the Ca2 site from silicocarnotite, and one-third of the Ca2 site from HAp becomes the Ca1 site in silicocarnotite, whereas the two other thirds of the Ca2 site from HAp become the Ca3 site in silicocarnotite.

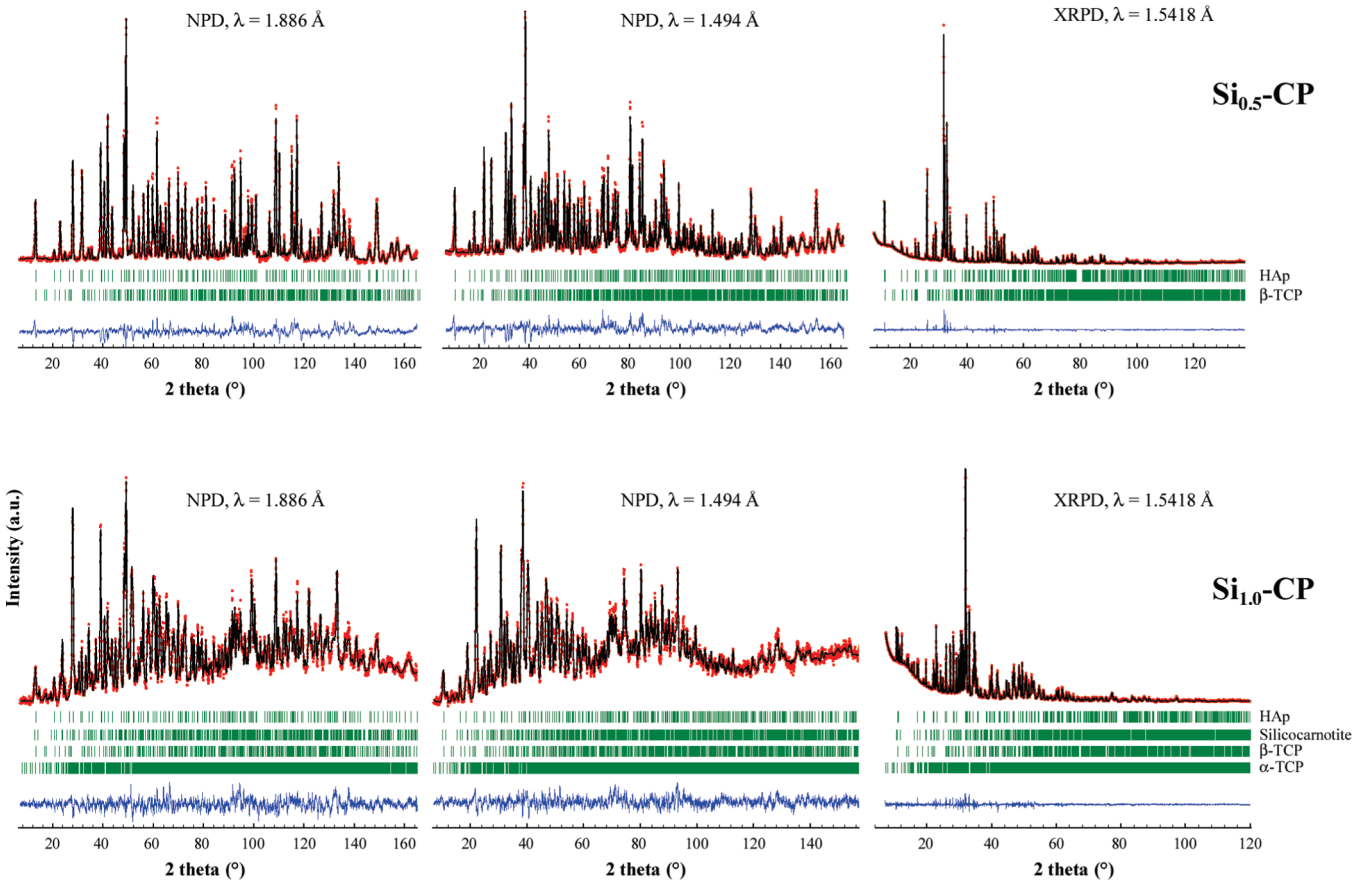

Figure 1. Rietveld plots from joint refinements on samples $Si_{0.5}$-CP (top) and $Si_{1.0}$-CP (bottom): neutron powder diffraction with λ = 1.886 Å (left), neutron powder diffraction with λ = 1.494 Å (middle), and X-ray powder diffraction with λ = 1.5418 Å (right). Experimental (red dots) and calculated (black lines) patterns, difference curves (blue lines), and Bragg peak positions (green ticks) for HAp, silicocarnotite, β-TCP and α-TCP are represented.

3.4. Raman Spectroscopy. Raman spectra recorded with the 10× objective represent the whole samples (Figure 4). The four modes of vibration of phosphate tetrahedra are observed in the spectral range 200−1300 cm^{-1} (the intense ν_1 mode around 960 cm^{-1}, the ν_2 modes around 450 cm^{-1}, the ν_3 modes around 1050 cm^{-1}, and the ν_4 modes around 600 cm^{-1}). The central inset in Figure 4 shows the detail corresponding to the intense ν_1 mode — the $[PO_4]$ symmetric stretching mode. Three main ν_1 components are observed at 955, 962, and 973 cm^{-1} for the three samples. Spectra recorded from samples $Si_{0.0}$-CP and $Si_{0.5}$-CP allow assignment of the 962 cm^{-1} component to HAp (the main phase for both samples) and the two 955 and 973 cm^{-1} components to β-TCP. These ν_1 assignments for HAp and β-TCP have been already described in the literature.[12,52−59] $Si_{1.0}$-CP spectrum presents also the four modes of vibration (from phosphate) at about the same positions but in a more complicated manner due to the presence of four calcium phosphate phases (having all isolated phosphate tetrahedron only). New bands appear in the silicate-containing samples at 893 cm^{-1} for $Si_{0.5}$-CP and at 847 cm^{-1} for $Si_{1.0}$-CP. These new bands are attributed to silicate Si−O symmetric stretching. Position around 850−900 cm^{-1} corresponds to isolated $Si[Q^0]$[60−62] in agreement with phosphate substitution. Absence of $Si[Q^3]$ and $Si[Q^4]$ signals confirms the absence of amorphous silica-gel. Spectral range relative to hydroxyl stretching (Figure 4 right) shows (1) an important decrease of the OH band intensity when silicate are incorporated in agreement with the mineralogical composition (due to the decrease of the HAp weight percent), (2) a broadening of the band as usually observed in substituted HAp,[12] and (3) the absence of new OH^- vibration when silicon is incorporated (indicating no deep modification of hydroxyl neighborhood when silicate is inserted). Carbonate vibration was not observed (either the A type with ν_1 $[CO_3^{2-}]$ at 1107 cm^{-1}, or the B type with ν_1 $[CO_3^{2-}]$ at 1070 cm^{-1})[55] in agreement with the high temperature of calcinations of 1100 °C.

Raman spectra recorded with the 100× magnification (resolution ∼1 μm × 1 μm) allow discrimination of selective regions in the samples enriched in one or another phases (see ν_1 bands in Figure 5). The spectrum a2 in Figure 5 corresponds to a β-TCP lightly enriched region in sample $Si_{0.5}$-CP. A band with very weak intensity is observed at 847 cm^{-1} that is not resolved in the whole $Si_{0.5}$-CP spectrum. This band can be assigned to the weak silicate insertion into β-TCP. The spectra b2, b3, and b4, respectively, in Figure 5 are attributed to HAp, silicocarnotite, and β-TCP, respectively, enriched regions in sample $Si_{1.0}$-CP. α-TCP enriched regions are difficult to discriminate because the main ν_1 componant of α-TCP superimpose with HAp and β-TCP (976 and 964 cm^{-1}).[57] The silicocarnotite phase is then characterized by the main component at 954 cm^{-1} (see spectrum b3 in Figure 5). All the spectra recorded for $Si_{1.0}$-CP sample present a silicate signal at 847 cm^{-1}, whatever the enriched region. The spectrum b3 which is attributed to a silicarnotite enriched region presents the most intense silicate vibration at 847 cm^{-1}. The spectrum b2, attributed to a HAp enriched region, presents also

dx.doi.org/10.1021/cg200587s |*Cryst. Growth Des.* 2011, 11, 4017–4026

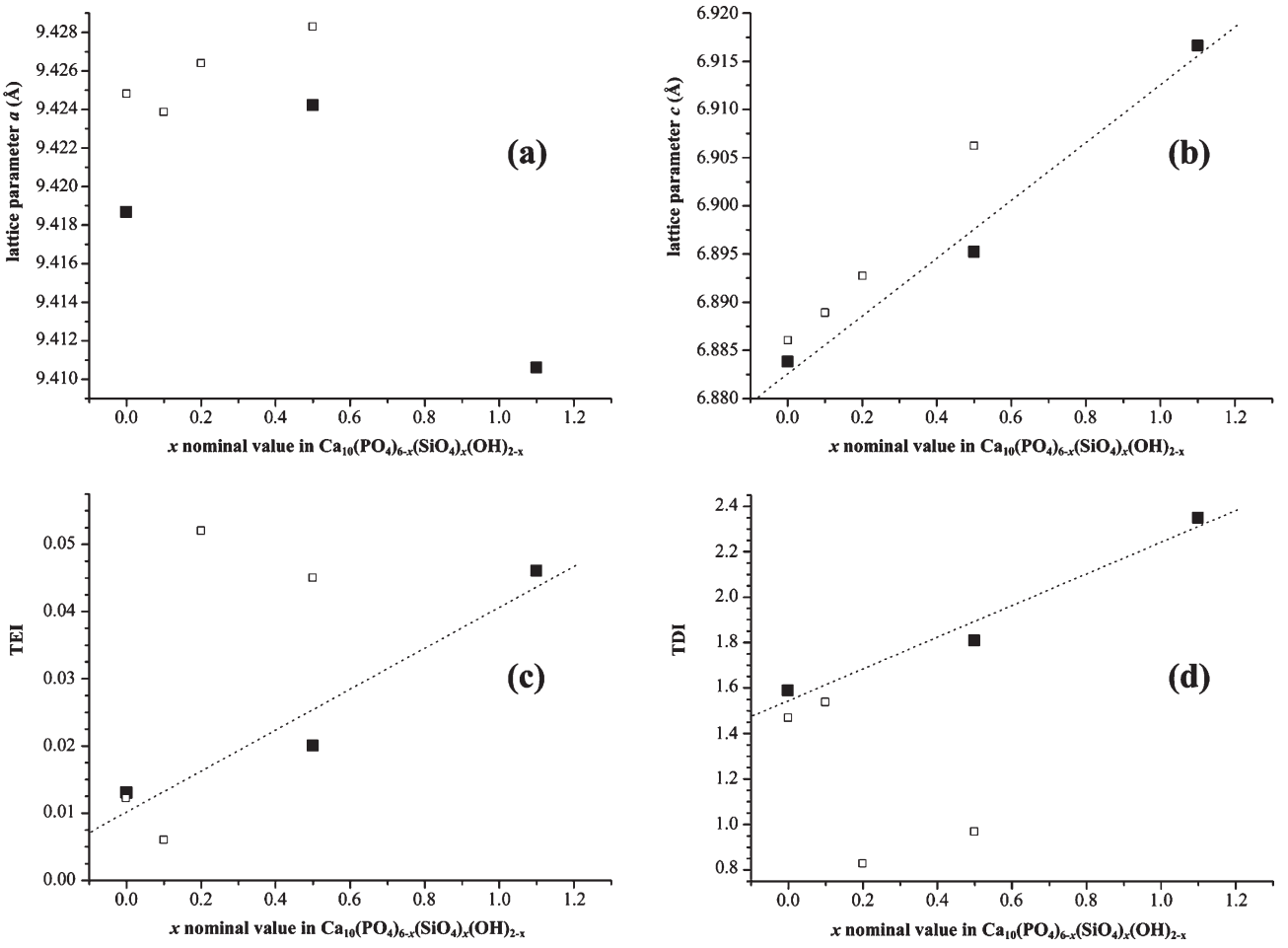

Figure 2. Evolution of the lattice parameters *a* (panel a) and *c* (panel b), the tehtrahedral elongation index TEI (panel c), and tetrahedral distortion index TDI (panel d) as a function of the *x* nominal value $Ca_{10}(PO_4)_{6-x}(SiO_4)_x(OH)_{2-x}$ (errors bars are within the symbols). Full square symbols relate values from the present study; small opened square symbols correspond to the previous study.[30] Dotted lines are linear fitting of full square symbols (present study).

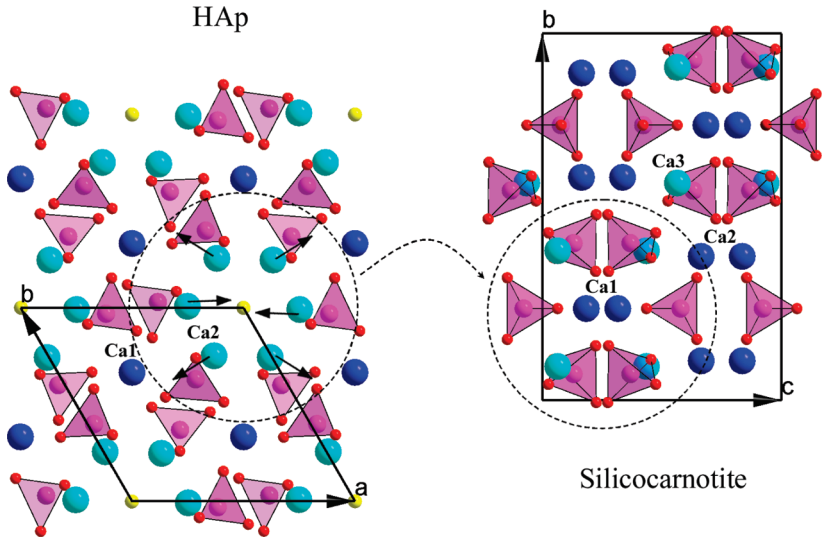

Figure 3. Structural representation of HAp and silicocarnotite: pink tetrahedra correspond to phosphate/silicate tetrahedra, blue spheres (dark blue and cyan) correspond to calcium cations, and yellow spheres correspond to hydroxyl anions (O4 site). Arrows in the HAp structure relate calcium moving induced when emptying of the hydroxyl hexagonal channel to obtain the silicocarnotite structure. Ca labels refer to a structure description of HAp[43] and of silicocarnotite.[46]

dx.doi.org/10.1021/cg200587s |*Cryst. Growth Des.* 2011, 11, 4017–4026

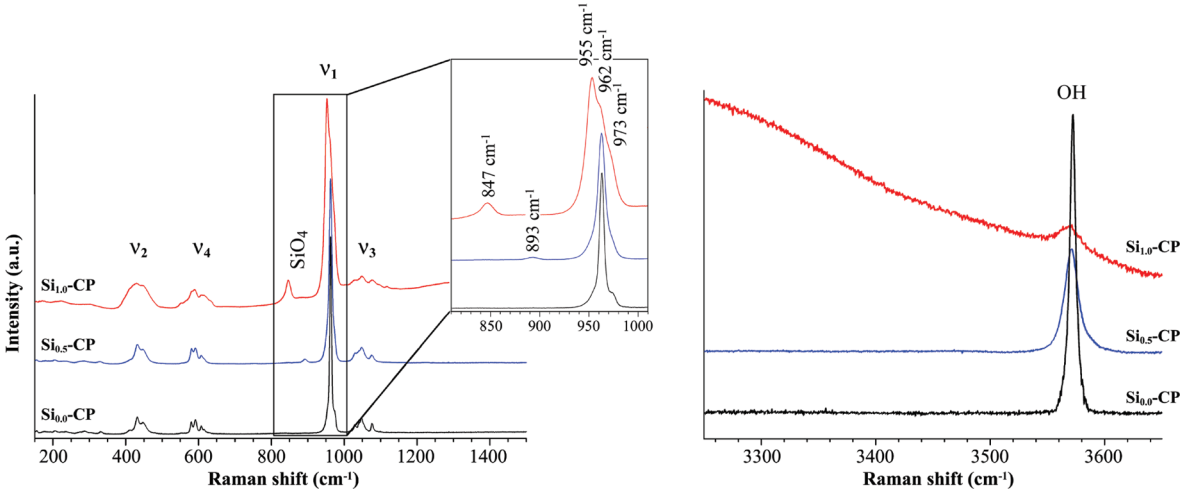

Figure 4. Raman spectra recorded with the 10× objective for the three Si_x-CP ($x = 0.0, 0.5, 1.0$) samples from spectral ranges 200−1300 cm^{-1} relative to phosphate modes of vibration (left) and 3250−3650 cm^{-1} relative to hydroxyl stretching (right). Central inset shows detail corresponding to the intense ν_1 mode of $[PO_4]$ and the stretching mode of $[SiO_4]$.

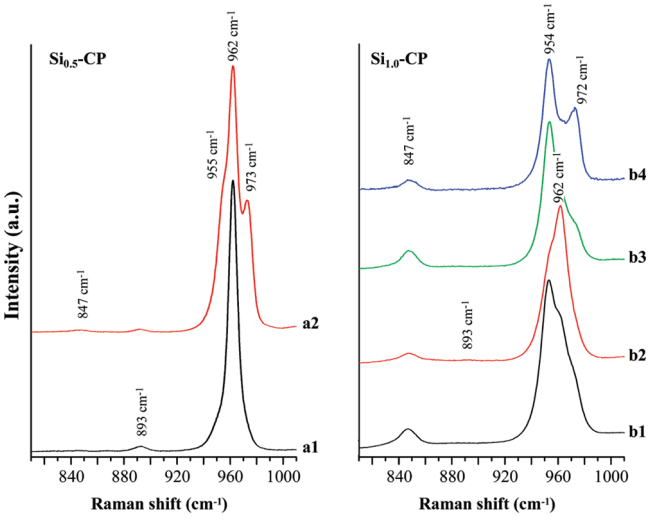

Figure 5. Raman spectral range 810−1010 cm^{-1} recorded with the 10× objective on $Si_{0.5}$-CP (a1) and $Si_{0.5}$-CP (b1), and Raman spectra recorded with the 100× objective on selected regions: enriched with β-TCP in $Si_{0.5}$-CP (a2), enriched with HAp in $Si_{1.0}$-CP (b2), enriched with silicocarnotite in $Si_{1.0}$-CP (b3), and enriched with β-TCP in $Si_{1.0}$-CP (b4).

this silicate signal at 847 cm^{-1} and also an extremely weak signal at 893 cm^{-1} (corresponding to the silicate signal observed in the $Si_{0.5}$-CP sample). This indicates that the silicate vibration from HAp evolves when passing from the $Si_{0.5}$-CP sample to $Si_{1.0}$-CP sample, i.e., when passing from HAp containing a relatively large OH^- amount ($Ca_{10}(PO_4)_{5.5(2)}(SiO_4)_{0.5(2)}(OH)_{1.36(4)}O_{0.58(3)}\square_{0.06(2)}$ in Table 3) to HAp containing a low amount of OH^- and large amount of hexagonal channel vacancies ($Ca_{10}(PO_4)_{4.9(2)}(SiO_4)_{1.1(2)}(OH)_{1.0(1)}O_{0.66(7)}\square_{0.34(4)}$ in Table 3). This evolution should be explained by the formation of hydrogen bonding between OH^- and $[SiO_4]$ as previously described for Si-Hap.[30] The silicate signal at 847 cm^{-1} is attributed to isolated Si[Q^0] and is not phase dependent, whereas the silicate signal at 893 cm^{-1} is attributed to the $[SiO_4](OH)_2$ entity, in agreement with an upshift toward the Si[Q^1] region[62] only present in the HAp phase with sufficient OH^- and low quantity of hydroxyl vacancies to ensure hydrogen bonding.

4. DISCUSSION

Low weight percents of β-TCP in both $Si_{0.0}$-CP and $Si_{0.5}$-CP samples are explained by the experimental Ca/P, or Ca/(P + Si), ratio close to the targeted 1.67 value which stabilizes the HAp compound (Table 1). The low quantity of β-TCP is formed during the high temperature treatment at 1100 °C. The as-prepared powders before heat treatment were composed of nanocrystalline hydroxyapatite only.[30] The quite similar lattice parameters for β-TCP in both $Si_{0.0}$-CP and $Si_{0.5}$-CP samples indicate that the HAp phase incorporates almost the whole silicon content in the $Si_{0.5}$-CP sample, forming Si-HAp. Thus, the maximal silicon amount that can substitute phopshate in HAp is not reached in $Si_{0.5}$-CP, i.e., is above 1.41 wt % (wt %) of silicon. Mixture of Si-HAp and silicocarnotite in the $Si_{1.0}$-CP sample allows the determination of the maximal insertion of Si into HAp structure: the maximal x value (x_{max}) for the hexagonal Si-HAp phase. Joint Rietveld refinement indicates the value $x_{max} = 1.1$ corresponding to the refined composition $Ca_{10}(PO_4)_{4.9(2)}(SiO_4)_{1.1(2)}(OH)_{1.0(1)}O_{0.66(7)}\square_{0.34(4)}$ (about half of the x value needed to form silicocarnotite). The $x_{max} = 1.1$ corresponds to 3.11 Si wt % in HAp, in between the previously reported maximal Si insertion values (1.6 Si wt % for Si-HAp prepared by aqueous precipitation method[27] and 4.0 Si wt % for Si-HAp prepared by the hydrothermal method).[32] The $x_{max} = 1.1$ value is close to the value determined by Palard et al. (single phase Si-HAp sample for $x \leq 1$).[26] $Ca_{10}(PO_4)_{6-x}(SiO_4)_x(OH)_{2-x}$ general formula corresponds to hexagonal Si-HAp for $0 \leq x \leq 1.1$ and to orthorhombic silicocarnotite for $x = 2$.

The Si-HAp phase from $Si_{1.0}$-CP sample shows a decrease of the OH^- population counterbalanced by the simultaneous increase of the O^{2-} population and mainly the oxygen vacancies. Such a decrease of the hydroxyl population when substituting silicate in HAp has already been described,[36,63,64] and the concomitent increases for O^{2-} population and hydroxyl vacancies have already been observed in our previous study.[30] The

dx.doi.org/10.1021/cg200587s |Cryst. Growth Des. 2011, 11, 4017–4026

hydroxyl thermal displacement parameter increases when substituting silicate (Table 3), as already described by Arcos et al.,[36] indicating the disorder increase around the HAp hydroxyl site. In the same way the observed decrease of the hydroxyl interatomic distance (see d_{O-H} in Table 3) indicates statistic disorder around the O4 site and corresponds to an average location of oxygen from hydroxyl and O^{2-}. Vacancies along the hexagonal hydroxyl channel indicate the following mechanism is actually present during silicate incorporation:

$$PO_4^{3-} + OH^- \leftrightarrow SiO_4^{4-} + \square_{OH}$$

Nevertheless partial hydroxyl loss in HAp can be simply achieved during heat treatment above 850 °C forming oxy-hydroxyapatite for undoped HAp,[17,65] and cannot explain by itself the charge balance. The observed unit cell negative elementary charge continuously increases when silicon is incorporated: −0.54, −1.02, and −1.42 (elementary charge), respectively, for $Si_{0.0}$-CP, $Si_{0.5}$-CP, and $Si_{1.0}$-CP, respectively. Occupancies related to the hydroxyl site (O4 and H1 sites) were refined and calcium occupancies converged to unity. Only a decrease of the phosphate/silicate occupancy parameters can offset the exess of negative charges, corresponding to a phosphate/silicate deficient Si-HAp. Refinement of the global occupancy for the phosphate/silicate site in the HAp structure was not concievable during Rietveld treatments without extremely strong correlations (leading to erroneous results and misinterpretations). When considering the refined unit cell elementary charges, the following chemical composition were calculated to reach electroneutrality: $Ca_{10}(PO_4)_{5.82}(\square_T)_{0.18}(OH)_{1.38}O_{0.58}\square_{0.04}$ for $Si_{0.0}$-CP, $Ca_{10}(PO_4)_{5.20}(SiO_4)_{0.47}(\square_T)_{0.33}(OH)_{1.36}O_{0.58}\square_{0.06}$ for $Si_{0.5}$-CP and $Ca_{10}(PO_4)_{4.54}(SiO_4)_{1.02}(\square_T)_{0.45}(OH)_{1.00}O_{0.66}\square_{0.34}$ for $Si_{1.0}$-CP, with $(\square_T)$ the tetrahedral phosphate/silicate vacancies and $\square$ the hydroxyl/oxide vacancies. The calculated chemical composition of HAp in the $Si_{0.0}$-CP sample falls within the standard deviations of the refined composition. The quantity of phosphate/silicate vacancies increases with the quantity of silicate inserted in HAp. The role of carbonate in the silicate incorporation into Si-HAp has been described by Palard et al.[26] Vacancies in the phosphate/silicate site can be explained by the presence of type B carbonate in the as-prepared samples according to the following mechanism:

$$2PO_4^{3-} \leftrightarrow SiO_4^{4-} + CO_3^{2-}$$

The type B carbonates are subsequently evacuated (around 800 °C) during the heat treatment with CO_2 evacuation from the phosphate/silicate site and with the displacing of the remaining O^{2-} from the phosphate/silicate site (vacancy formation on the phosphate/silicate site) to the hexagonal channel according to the mechanism:

$$SiO_4^{4-} + CO_3^{2-} \leftrightarrow SiO_4^{4-} + O^{2-}$$

Silicocarnotite of composition $Ca_5(PO_4)_2SiO_4$ corresponds in terms of chemical formula to $Ca_{10}(PO_4)_{6-x}(SiO_4)_x(OH)_{2-x}$ with $x = 2$ but has a different crystallographic structure. This indicates that Si-HAp cannot incorporate the maximal physical silicate content ($x = 2$). Certainly the charge compensation mechanisms, or more simply the emptying of the hydroxyl hexagonal channel (which is certainly the structural destabilizing feature, already supposed by Dickens and Brown),[46] explain the change from the hexagonal symmetry for Si-HAp ($0 \le x \le 1.1$) to the orthorhombic symmetry for silicocarnotite ($x = 2$), which is the previously described reorganization of the crystallographic structure (see section 3.3).

5. CONCLUSION

Biphasic calcium phosphate (BCP) ceramic has been obtained for a phosphate substitution level of about 8 mol % (i.e., for a nominal composition of $Ca_{10}(PO_4)_{6-x}(SiO_4)_x(OH)_{2-x}$ with $x = 0.5$), whereas multiphase calcium phosphate ceramic was obtained for a phosphate substitution level of about 15 mol % (i.e., for a nominal composition of $Ca_{10}(PO_4)_{6-x}(SiO_4)_x(OH)_{2-x}$ with $x = 1.0$). The multiphase ceramic contains HAp, silicocarnotite, β-TCP, and α-TCP. Silicate anions have been detected in the four phases: weak quantity for β-TCP (too low to be estimated) and measurable quantities for the three other phases. The maximal quantity of silicate insertion in HAp is obtained with a phosphate substitution level of 18.3 mol % corresponding to the refined composition $Ca_{10}(PO_4)_{4.9(2)}(SiO_4)_{1.1(2)}(OH)_{1.0(1)}O_{0.66(7)}\square_{0.34(4)}$, or calculated composition $Ca_{10}(PO_4)_{5.20}(SiO_4)_{0.47}(\square_T)_{0.33}(OH)_{1.36}O_{0.58}\square_{0.06}$ when considering electroneutrality. The refined composition of silicocarnotite is $Ca_5(PO_4)_{1.9(2)}(SiO_4)_{1.1(2)}$, very close to the normal $Ca_5(PO_4)_2SiO_4$ composition, with silicon substitution in both phosphorus crystallographic sites. The estimated composition of Si-α-TCP is $Ca_3(PO_4)_{1.875}(SiO_4)_{0.125}$ (determined by considerations on lattice parameters only) which corresponds to the previously published maximal level of silicate insertion into α-TCP.

The mechanism of silicate insertion into the HAp structure appeared to be complex and multiple. Nevertheless, it appears that silicate insertion, phosphate/silicate vacancies, and hydroxyl vacancies are intimately linked. The phosphate to silicate substitution is mainly realized according to the following two mechanisms:

$$PO_4^{3-} + OH^- \leftrightarrow SiO_4^{4-} + \square_{OH}$$

$$2PO_4^{3-} \overset{RT}{\leftrightarrow} SiO_4^{4-} + CO_3^{2-} \overset{\approx 800\ ^\circ C,\ CO_2\uparrow}{\leftrightarrow} SiO_4^{4-} + O^{2-} + (\square_T)$$

The first mechanism explains the formation of hydroxyl vacancies when silicate ions are incorporated, leading to the composition $Ca_{10}(PO_4)_{6-x}(SiO_4)_x(OH)_{2-x}$. And the second mechanism, involving a type B carbonate in the as-prepared powders, explains the calculated phosphate/silicate vacancies, noted $(\square_T)$, to reach electroneutrality for Si-HAp (due to carbonate decomposition during the heat treatment) and compensate partially the hydroxyl vacancies into the hexagonal channel, leading to the composition $Ca_{10}(PO_4)_{6-2y}(SiO_4)_y(CO_3)_y(OH)_2$. The general chemical composition after heat treatment is $Ca_{10}(PO_4)_{6-x-2y}(SiO_4)_{x+y}(\square_T)_y(OH)_{2-x}O_y\square_{x-y}$ with $(\square_T)$ the tetrahedral phosphate/silicate vacancies and $\square$ the hydroxyl/oxide vacancies. The hydroxyl vacancies formation into the hexagonal channel of HAp structure is destabilizing and leads to the formation of silicocarnotite. Silicocarnotite should be considered as a polymorph of highly silicate-substituted HAp $Ca_{10}(PO_4)_{6-x}(SiO_4)_x(OH)_{2-x}$ with $x = 2.0$, i.e., $Ca_5(PO_4)_2SiO_4$.

AUTHOR INFORMATION

Corresponding Author

*E-mail: guillaume.renaudin@ensccf.fr. Tel.: 00 33 4 73 40 73 36. Fax: 00 33 4 73 40 70 95.

■ ACKNOWLEDGMENT

This work was supported by ANR under Project NANOSHAP (ANR-09-BLAN-0120-03). This work is partially based on the experiments carried out at the Swiss spallation neutron source SINQ at the Paul Scherrer Intitut, Villigen, Switzerland.

■ REFERENCES

(1) Dahl, S. G.; Allain, P; Marie, P. J.; Mauras, Y.; Boivin, G.; Ammann, P.; Tsouderos, Y.; Delmas, P. D.; Christiansen, C. *Bone* **2001**, *28* (4), 446–453.
(2) Lagier, R.; Baud, C. A. *Pathol. Res. Pract.* **2003**, *199* (5), 329–335.
(3) Lee, R. S.; Kayser, M. V.; Ali, S. Y. *J. Anat.* **2006**, *208* (1), 13–19.
(4) Elliot, J. C. *Structure and Chemistry of the Apatites and Other Calcium Orthophosphates*; Elsevier: Amsterdam, The Netherlands, 1994.
(5) Hench, L. L. *J. Am. Ceram. Soc.* **1991**, *74* (7), 1487–1510.
(6) Oonishi, H.; Hench, L. L.; Wilson, J.; Sugihora, F.; Tsuji, E.; Matsuura, M.; Kin, S.; Yamamoto, T.; Mizokawa, S. *J. Biomed. Mater. Res.* **2000**, *51* (1), 37–46.
(7) Ducheyne, P.; Qiu, Q. *Biomaterials* **1999**, *20* (23−24), 2287–2303.
(8) Vallet-Regi, M. *J. Chem. Soc., Dalton Trans.* **2001**, *2*, 97–108.
(9) Renaudin, G.; Laquerriere, P.; Filinchuk, Y.; Jallot, E.; Nedelec, J. M. *J. Mater. Chem.* **2008**, *18* (30), 3593–3600.
(10) Renaudin, G.; Jallot, E.; Nedelec, J. M. *J. Sol-Gel Sci. Technol.* **2009**, *51* (3), 287–294.
(11) Gomes, S.; Renaudin, G.; Jallot, E.; Nedelec, J. M. *Appl. Mater. Interfaces* **2009**, *1* (2), 505–513.
(12) Gomes, S.; Nedelec, J. M.; Jallot, E.; Sheptyakov, D.; Renaudin, G. *Chem. Mater.* **2011**, *23*, 3072–3085.
(13) LeGeros, R. Z. *Arch. Oral Biol.* **1974**, *20*, 63–71.
(14) Mackie, P. E.; Elliot, J. C.; Young, R. A. *Acta Crystallogr. B* **1972**, *28*, 1840–1848.
(15) Elliot, J. C.; Bonel, G.; Trombe, J. C. *J. Appl. Crystallogr.* **1980**, *13*, 618–621.
(16) DeBoer, B. G. *Acta Crystallogr. B* **1991**, *47*, 683–692.
(17) Serret, A.; Cabanas, M. V.; Vallet-Regi, M. *Chem. Mater.* **2000**, *12* (12), 3836–3841.
(18) Gibson, I. R.; Best, S. M.; Bonfield, W. *J. Biomed. Mater. Res.* **1999**, *44*, 422–428.
(19) Vallet-Regí, M.; Arcos, D. *J. Mater. Chem.* **2005**, *15*, 1509–1516.
(20) Arcos, D.; Sanchez-Salcedo, S.; Izquierdo-Barba, I.; Ruiz, L.; González-Calbet, J.; Vallet-Regí, M. *J. Biomed. Mater. Res. Part A* **2006**, *78A* (4), 762–771.
(21) Pietak, A. M.; Reid, J. W.; Stott, M. J.; Sayer, M. *Biomaterials* **2007**, *28*, 4023–4032.
(22) Thian, E. S.; Huang, J.; Best, S. M.; Barber, Z. H.; Brooks, R. A.; Rushton, N.; Bonfield, W. *Biomaterials* **2006**, *27*, 2692–2698.
(23) Carlisle, E. M. *Science* **1970**, *167*, 279–280.
(24) Bohner, M. *Biomaterials* **2009**, *30*, 6403–6406.
(25) Habibovic, P.; Barralet, J. E. *Acta Biomater.* **2011**, *7*, 3013–3026. DOI:10.1016/j.actbio.2011.03.027.
(26) Palard, M.; Champion, E.; Foucaud, S. *J. Solid State Chem.* **2008**, *181*, 1950–1960.
(27) Balas, F.; Perez-Pariente, J.; Vallet-Regi, M. *J. Biomed. Mater. Res.* **2003**, *66A*, 364–375.
(28) Gibson, I. R.; Best, S. M; Bonfield, W. *J. Am. Ceram. Soc.* **2002**, *85* (11), 2771–2777.
(29) Leventouri, T.; Bunaciu, C. E.; Perdikatsis, V. *Biomaterials* **2003**, *24* (23), 4205–4211.
(30) Gomes, S.; Renaudin, G.; Mesbah, A.; Jallot, E.; Bonhomme, C.; Babonneau, F.; Nedelec, J. M. *Acta Biomater.* **2010**, *6*, 3264–3274.
(31) Gasquère, G.; Bonhomme, C.; Maquet, J.; Babonneau, F.; Hayakawa, S.; Kanaya, T.; Osaka, A. *Magn. Reson. Chem.* **2008**, *46*, 342–346.
(32) Tang, X. L.; Xiao, X. F.; Liu, R. F. *Mater. Lett.* **2005**, *59*, 3841–3846.
(33) Ruys, A. J. *J. Australas. Ceram. Soc.* **1993**, *29*, 71–80.
(34) Tanizawa, Y.; Suzuki, T. *J. Chem. Soc. Faraday Trans.* **1995**, *91*, 3499–3503.
(35) Boyer, L.; Carpena, J.; Lacout, J. L. *Solid State Ionics* **1997**, *95*, 121–129.
(36) Arcos, D.; Rodríguez-Carvajal, J.; Vallet-Regí, M. *Solid State Sci.* **2004**, *6*, 987–994.
(37) Arcos, D.; Rodríguez-Carvajal, J.; Vallet-Regí, M. *Chem. Mater.* **2004**, *16*, 2300–2308.
(38) Gibson, I. R.; Huang, J.; Best, S. M.; Bonfield, W. In *Bioceramics*; Ohgushi, H.; Hastings, G. W.; Yoshikawa, T., Eds.; World Scientific: Singapore, 1999; Vol. 12, pp 191−194.
(39) Porter, A. E; Patel, N.; Skepper, J. N.; Best, S. M.; Bonfield, W. *Biomaterials* **2003**, *24*, 4609–4620.
(40) Kim, S. R.; Lee, J. H.; Kim, Y. T.; Riu, D. H.; Jung, S. J.; Lee, Y. J.; Chung, S. C.; Kim, Y. H. *Biomaterials* **2003**, *24*, 1389–1398.
(41) Fischer, P.; Frey, G.; Koch, M.; Könnecke, M.; Pomjakushin, V.; Schefer, J.; Thut, R.; Schlumpf, N.; Bürge, R.; Greuter, U.; Bondt, S.; Berruyer, E. *Physica B* **2000**, *276*, 146–148http://sinq.web.psi.ch/sinq/instr/hpt/index.html.
(42) Rodríguez-Carvajal, J. *Physica B* **1993**, *192*, 55–69.
(43) Kay, M. I.; Young, R. A.; Posner, A. S. *Nature* **1964**, *204*, 1050–1052.
(44) Yashima, M.; Sakai, A.; Kamiyama, T.; Hoshikawa, A. *J. Solid State Chem.* **2003**, *175*, 272–277.
(45) Mathew, M.; Schroeder, L. W.; Dickens, B.; Brown, W. E. *Acta Crystallogr. B* **1977**, *33*, 1325–1333.
(46) Dickens, B.; Brown, W. E. *Tschermaks Mineral. Petrogr. Mitt.* **1971**, *16*, 1–27.
(47) McCusker, L. B.; Von Dreele, R. B.; Cox, D. E.; Louër, D.; Scardi, P. *J. Appl. Crystallogr.* **1999**, *32*, 36–50.
(48) Nurse, R. W.; Welsh, J. H.; Gutt, W. *J. Chem. Soc.* **1959**, 1077–1083.
(49) Reid, J. W.; Tuck, L.; Sayer, M.; Fargo, K.; Hendry, J. A. *Biomaterials* **2006**, *27*, 2916–2925.
(50) Fix, W.; Heymann, H.; Heinke, R. *J. Am. Ceram. Soc.* **1969**, *52* (6), 346–347.
(51) Keppler, U. *Neues Jahrb. Mineral., Monatsh.* **1968**, *9*, 320–331.
(52) Blakeslee, K. C., Sr.; Condrate, R. A. *J. Am. Ceram. Soc.* **1971**, *54* (11), 559–563.
(53) De Aza, P. N.; Santos, C.; Pazo, A.; De Aza, S.; Cuscó, R.; Artús, L. *Chem. Mater.* **1997**, *9*, 912–915.
(54) Cuscó, R.; Guitián, F.; De Aza, S.; Artús, L. *J. Eur. Ceram. Soc.* **1998**, *18*, 1301–1305.
(55) Penel, G.; Leroy, G.; Rey, C.; Bres, E. F. *Calcif. Tissue Int.* **1998**, *63*, 475–481.
(56) Penel, G.; Leroy, N.; Van Landuyt, P.; Flautre, B.; Hardouin, P.; Lemaître, J.; Leroy, G. *Bone* **1999**, *25* (2), 81S–84S.
(57) Jillavenkatesa, A., Sr.; Condrate, R. A. *Spectrosc. Lett.* **1998**, *31* (8), 1619–1634.
(58) Zou, S.; Huang, J; Best, S.; Bonfield, W. *J. Mater. Sci. Mater. Med.* **2005**, *16*, 1143–1148.
(59) Quillard, S.; Paris, M.; Deniard, P.; Gildenhaar, R.; Berger, G.; Obadia, L; Bouler, J.-M. *Acta Biomater.* **2011**, *7* (4), 1844–52.
(60) McMillan, P. *Amer. Mineral.* **1984**, *69*, 622–644.
(61) Colomban, P. *Actual. Chim.* **2003**, *261*, 12–17.
(62) Renaudin, G.; Russias, J.; Leroux, F.; Cau-dit-Coumes, C.; Frizon, F. *J. Solid State Chem.* **2009**, *182*, 3320–3329.
(63) Aminiam, A.; Solati-Hasjin, M.; Bakhshi, F.; Farzadi, A. *Ceram. Trans.* **2010**, *218*, 67–74.
(64) Aminiam, A.; Solati-Hasjin, M.; Samadikuchaksaraei, A.; Bakhshi, F.; Gorjipour, F.; Farzadi, A.; Moztarzadeh, F.; Schucker, M. *Ceram. Int.* **2011**, *37* (4), 1219–1229.
(65) Trombe, J. C.; Montel, G. *J. Inorg. Nucl. Chem.* **1978**, *40* (1), 23–26.